Desalination and Water Treatment
www.deswater.com

doi: 10.5004/dwt.2023.29981

311 (2023) 196–208
November

Adsorption of tetrakis(hydroxymethyl)phosphonium chloride on pomelo peel biochar and its antimicrobial ability

Zhuannian Liu[a,*], Yue Li[a], Junnan Luo[a], Changshun Sun[b], Luncong Deng[a], Rui Zhou[a]

[a]*College of Geology and Environment, Xi'an University of Science and Technology, Xi'an 710054, China, emails: liuzhuannian@163.com (Z. Liu), 1165748150@qq.com (Y. Li), 923553218@qq.com (J. Luo), 2197571932@qq.com (L. Deng), 1693376060@qq.com (R. Zhou)*
[b]*Shaanxi Provincial Research Academy of Environmental Sciences, Xi'an 710061, China, email: 478456578@qq.com*

Received 24 January 2023; Accepted 7 September 2023

ABSTRACT

In this study, potassium hydroxide (KOH), aluminum chloride ($AlCl_3$), and zinc chloride ($ZnCl_2$) were co-pyrolyzed with pomelo peel biomass (according to different pyrolysis conditions, abbreviated in order as KOH-BC, $AlCl_3$-BC, and $ZnCl_2$-BC) to enhance the original biochar (BC) adsorption performance of an emerging contaminant tetrakis(hydroxymethyl)phosphonium chloride (THPC). The adsorption experiments indicated that the adsorption capacity for THPC of KOH-BC reached 438 $mg \cdot g^{-1}$, which showed much higher adsorption properties than those of BC (239.6 $mg \cdot g^{-1}$), $AlCl_3$-BC (301.6 $mg \cdot g^{-1}$) and $ZnCl_2$-BC (278.9 $mg \cdot g^{-1}$) due to its better developed pore structures. The adsorption process of THPC by BC, KOH-BC, $AlCl_3$-BC, and $ZnCl_2$-BC, a spontaneous endothermic process that had been analyzed, according with the second-order kinetic model and Langmuir isotherm model. And the adsorption mechanisms of THPC removal (i.e., pore filling, cation-π interaction, hydrogen bonding, and ion exchange) were summarized. Targeting *Escherichia coli*, the antibacterial activity of BC (THPC-BC) and KOH-BC (THPC-KOH-BC) of THPC after adsorption was explored. Antibacterial activity experiments have shown that THPC-BC and THPC-KOH-BC could effectively inhibit the growth of *E. coli*. Therefore, BC and modified BC can not only be used to remove THPC but also be recycled for secondary utilization, which provides a novel idea for the emission reduction and resource recycling of THPC with great practical value.

Keywords: Adsorption; Biochar activation; Tetrakis(hydroxymethyl)phosphonium chloride; *Escherichia coli*; Sterilization; Water treatment

1. Introduction

With the development of industry, it is more challenging to treat refractory organic compounds in industrial wastewater [1]. Traces of novel organic chemicals have been detected in many aquatic environments (e.g., drugs, flame retardants, pesticides, endocrine disruptors, coatings, and cosmetic additives) [2], and organic compounds existing in the water environment cause serious harm to the ecological environment. For example, exposure to dyes may have adverse effects on human health, leading to anemia, skin diseases, permanent eye damage, and kidney blood bleeding [3]. Pesticide residues can contaminate soil, water sources, plants, etc., and accumulate through the food chain, thereby endangering the growth and reproduction of animals and plants. In addition, some pesticides are highly toxic and may endanger life if not completely treated [4]. Tetrakis(hydroxymethyl)phosphonium chloride (THPC), a novel organic compound in industrial organic phosphorus wastewater [5], is widely used as a flame retardant for fabrics [6], a chrome tanning agent in the leather industry, a descaling agent in the petroleum industry, a non-oxidizing

* Corresponding author.

bactericide in industrial water treatment and an oxygen scavenger in the medical industry [7]. THPC can be decomposed to PH_3 and formaldehyde in the water environment [8]. Further, highly toxic gases generated through PH_3 and formaldehyde are carcinogenic and mutagenic in humans [9,10]. Industrial wastewater, containing a large amount of THPC organic compounds, is discharged into environment, which can cause more harm to the ecological environment. Consequently, it is imperative to remove THPC from industrial wastewater.

Recently, the methods for removing organic phosphorus from wastewater have been varied, including adsorption [11], membrane filtration [12], photo-Fenton [11] and biological, etc. [13]. Adsorption is widely used due to its easy operation, excellent removal efficiency and low cost [14–16]. For example, urea modified activated carbon under high-temperature can optimize the pore structure of activated carbon and effectively improve its adsorption performance for dioxins [17], *in-situ* growth of Zn-Al LDH on polyaniline coated carbon spheres can effectively adsorb naproxen [18], the modification of magnetic graphite oxide (MGO) surface with lanthanum sulfide nanoparticles can effectively remove Pb^{2+} from wastewater [19], while these adsorbents are challenging to separate, expensive and unstable in acidic wastewater. Biochar, with its large surface area, large pore volume, abundance of resources and low price, is widely used to treat organic pollutants in aquatic environments [20,21]. Due to its finite specific surface area and underdeveloped pore structure, original biochar (BC) has limited adsorption performance. Chemical modification and metal oxide modification can enhance the pore volume and adsorption capacity of the original biochar, respectively [22]. Li et al. [23] used modified biochar impregnated with $KMnO_4$ and found it was successfully loaded with manganese oxide particles, which provided more adsorption sites and enhanced the adsorption of Cd^{2+}. In addition, modification of biochar with magnesium and aluminum [24] can enhance the specific surface area and promote the formation of highly developed pore structure, which is used for the treatment of eutrophic water. Because the acid–base modification can regulate the acidic functional groups, the adsorption capacities of NaOH and potassium hydroxide (KOH) activated biochar were significantly increased by 2.93 and 4.74 times, respectively [25].

Adsorbents after adsorption are usually disposed of by incineration, composting, regeneration, etc. [26]. Composting and incineration can cause secondary pollution in the environment. And regeneration is usually regenerated through chemical process, which is not only expensive but a disadvantageous influence on the environment. Thus, the secondary utilization of adsorbents after adsorption can relieve the hazard to environment. Nowadays, biochar has been used to adsorb Ag^+ and after adsorption, the biochar can also be used for producing novel value-added nanocomposite materials with antibacterial capability, which can successfully inhibit the growth of *Escherichia coli* [27–29]. According to literature reports, biochar is used to absorb phosphorus or phosphate in wastewater, and biochar after adsorption of phosphorus not only solves the problem of water eutrophication but also acts as fertilizer of plants to realize resource reuse [30–32].

E. coli is one of the sources of microbial contamination in the bottom of rivers and lakes, which increases the risk of water-borne diseases. There exists a dynamic balance between bottom sludge and upper water in rivers and lakes, while compared with the upper layers of water, the concentration of *E. coli* in the bottom sludge of the lake is higher [33]. At present, the main method to control *E. coli* pollution in water is to keep the concentration of *E. coli* in the water at a low level. However, the resuspension of sludge will increase the concentration of *E. coli* in the water over time. THPC, as a quaternary phosphonium salt, has an excellent bactericidal effect. In terms of the bactericidal characteristics of THPC, biochar is used as a carrier to absorb THPC and settled into the bottom sludge of rivers and lakes to kill *E. coli*. This is an effective method to reducing emission and resource utilization of the pollutant.

In conclusion, this study uses modified biochar to remove THPC and provides a new idea for efficient resource utilization by exploring the sterilization treatment of biochar on *E. coli* after adsorption of THPC from wastewater. The main objectives were: (1) to find a novel organic compound pollutant THPC; (2) to use pomelo peel as a raw material to make pure biochar (BC) and modified biochar (KOH-BC, $AlCl_3$-BC, and $ZnCl_2$-BC), and characterize through Brunauer–Emmett–Teller, scanning electron microscopy (SEM), Fourier-transform infrared spectroscopy (FTIR), and X-ray diffraction (XRD); (3) to compare the adsorption performance of THPC between the original biochar and modified ones, then reveal the adsorption mechanism; (4) to study the antibacterial activity of biochar on *E. coli* after the adsorption of THPC and explain the sterilization mechanism by using the sterilization kinetic model.

2. Materials and methods

2.1. Chemicals

Potassium hydroxide (KOH), aluminum chloride ($AlCl_3$), and zinc chloride ($ZnCl_2$) were purchased from the China Pharmaceutical Chemicals Co., Ltd., (China). Tetrakis(hydroxymethyl)phosphonium chloride ($C_4H_{12}ClO_4P$) was purchased from McLean Biochemical Technology Co., Ltd., (China). Soluble starch ($(C_6H_{10}O_5)_n$), iodine ($1/2I_2$) and sodium bicarbonate ($NaHCO_3$) were provided by Tianjin Kermel Chemical Reagent Co., Ltd., (China). Tryptone, agar powder and yeast extract powder were supplied from Beijing Aoboxing Biotechnology Co., Ltd., (China). All chemicals were of analytical grade.

2.2. Preparation of materials

The pomelo peel was washed three times with DI water, cut into long strips, dried, crushed into powder with a grinder, and sifted through a 200-mesh sieve. 4 g of pomelo peel powder and 1 g of KOH were mixed in a mortar and ground for 5 min, placed in a crucible boat for compaction and put in a tube furnace. The temperature was heated to 700°C at a rate of 5°C/min and pyrolyzed for 2 h under a N_2 flow. After that, it was washed to pH = 7 and dried for 12 h at 80°C, which was labeled as KOH-BC. With the same treatment process, the activators were replaced by $AlCl_3$

and $ZnCl_2$ to prepare $AlCl_3$-BC and $ZnCl_2$-BC (biochar (BC): without activator).

2.3. Characterization

The surface morphology was characterized by JSM-6710F scanning electron microscope of JEOL in Japan. The specific surface area and pore size of BC, KOH-BC, $AlCl_3$-BC and $ZnCl_2$-BC were measured by ASAP 2020 nitrogen physical adsorption instrument from USA. The crystal structure of the samples was observed by XD-3 X-ray diffractometer from Beijing Puxi General Instrument Co., Ltd., China. The surface chemical functional groups were analyzed by USA Perkin-Elmer 550S Fourier-transform infrared spectrometer. The zeta potential was measured by JS94H microelectrophore by adjusting the suspension of the sample with HCl and NaOH to 2, 3, 4, 5, 6, 7, 8 and 9 and then calculated through software.

2.4. Experiment on adsorption performance

2.4.1. Adsorption kinetics experiment

The adsorbent and THPC solution (200 mg·L^{-1}) were filtered at different shaking times (10, 30, 60, 120, 180, 240, 300, 360, 420, 480, 540, 720, and 1,080 min) and the concentration of the solution was measured after the samples were filtered.

2.4.2. Adsorption isotherm model

The adsorbent and THPC solutions of different concentrations (100, 200, 400, 600, and 1,000 mg·L^{-1}) were shaken for 12 h and the concentration of the solution was detected after the samples were filtered.

2.4.3. Adsorption thermodynamics

The adsorbent and THPC solutions were shaken for 12 h at different temperatures (298.15, 308.15, 318.15, 373.15, and 338.15 K). Then the concentration of the solution was detected after the samples were filtered.

2.4.4. Data analysis

After adsorption, the concentration of the filtrate was tested by the iodometric method [Eq. (1)].

$$C_{(\mathrm{THPC})} = \frac{C_{(I_2)} \times M_{(\mathrm{THPC})} \times \left(V_1 - V_0\right)}{V_{(\mathrm{THPC})}} \tag{1}$$

where $C_{(\mathrm{THPC})}$ is the concentration of THPC, mg·L^{-1}; $M_{(\mathrm{THPC})}$ is the relative molecular weight of THPC; V_1 is the volume of iodine standard solution consumed for titration of THPC solution, mL; V_0 is the volume of iodine standard solution consumed for titration blank, mL; $C_{(I_2)}$ is the concentration of iodine standard solution, mol·L^{-1}; $V_{(\mathrm{THPC})}$ is the volume of THPC solution, mL.

The adsorption capacity (q_e) of THPC was calculated through the Eq. (2):

$$q_e = \frac{\left(C_0 - C_e\right)V}{m} \tag{2}$$

where q_e is adsorption capacity of THPC, mg·g^{-1}; C_0 is the initial concentration of THPC, mg·L^{-1}; C_e is the concentration of THPC bringing into equilibrium, mg·L^{-1}; V is the volume of THPC solution, L; m is the mass of the samples.

2.5. Antimicrobial ability test

2.5.1. Preparation of antibacterial materials

0.5 g of BC and KOH-BC were put into 150 mL of THPC solution (1,000 mg·L^{-1}) in turn and shaken at 25°C 150 rpm for 12 h. After filtration, THPC-containing biochar was dried at 40°C (labelled as THPC-BC and THPC-KOH-BC).

2.5.2. Tested bacteria

THPC-BC and THPC-KOH-BC were tested for antibacterial ability with *E. coli* ATCC 25922.

2.5.3. Preparation of bacterial suspension

The bacteria were inoculated in 50 mL LB liquid medium with an inoculating loop, and shaken in shaking box at 37°C for 12 h, so that the absorbance measured by the spectrophotometer at 600 nm was between 0.5~0.6 (concentration was 5~6 × 10^8 CFU/mL), diluted to 10^{-5} times with sterile water (the concentration was 5~6 × 10^3 CFU/mL).

2.5.4. Effects of contact time on antibacterial activity

After 4 mg of THPC-BC and THPC-KOH-BC were contacted with 2 mL *E. coli* dilution for different time (10, 20, 30, 40, 60, and 90 min), 200 μL supernatant was taken and spread on the plate, which was put upside down in a constant temperature incubator at 37°C for 24 h, counting the number of bacterial colonies on the plate, adding the material without THPC and material without anything as a control.

3. Results and discussion

3.1. Characterization of biochar

The SEM image of BC, KOH-BC, $AlCl_3$-BC and $ZnCl_2$-BC are shown in Fig. 1. The irregular and uneven surface morphology of BC is illustrated in Fig. 1a, with wrinkles and no obvious pore structure to be observed, most of which were wrinkled and fragmented structures. The reason was that the organic substances such as cellulose and lignin in pomelo peel were decomposed during the carbonization process of BC [34], and the breakage of chemical bonds, accompanied by the release of volatiles, resulted in wrinkles and a few pores on BC. On the contrary, as shown in Fig. 1b, KOH-BC had an abundant, honeycomb-like pore structure due to the fact that during the pyrolysis, KOH reacted with the carbon precursors of the biomass to etch carbon fragments, and reacted with oxygen functional groups in the biomass. A large amount of gas was released during these reactions,

forming an abundant micropore–mesoporous structure, providing more adsorption sites for THPC [35]. As observed in Fig. 1c and d, compared with BC, $AlCl_3$-BC had deeper wrinkles, more pores, and alumina particles were produced on the surface. The SEM of $ZnCl_2$-BC was similar to $AlCl_3$-BC and the crystal particles on its surface were demonstrated as ZnO crystal particles in XRD detection.

As shown in Fig. 2, under low relative pressure (P/P_0 < 0.1), the adsorption capacities of BC, KOH-BC and $ZnCl_2$-BC increased rapidly, reaching the saturation value after a certain pressure, and there was no obvious hysteresis line. Depending on the classification of International Union of Pure and Applied Chemistry, the adsorption–desorption curves of BC and KOH-BC both had obvious characteristics of the type I isotherm [36,37], which was similar to the Langmuir adsorption isotherm, typically characterized in monolayer adsorption, with pore-filling as the main function of its adsorption. The adsorption–desorption curve of $AlCl_3$-BC revealed an obvious isotherm of type II, which appeared as an H_4 loop that showed an adsorbent mixed with micropores and mesopores.

As the specific surface area parameters could be seen from Table 1, compared with BC (261.47 $m^2 \cdot g^{-1}$), the specific surface area of KOH-BC (512.26 $m^2 \cdot g^{-1}$) and $ZnCl_2$-BC (306.53 $m^2 \cdot g^{-1}$) improved, while that of $AlCl_3$-BC (153.68 $m^2 \cdot g^{-1}$) reduced. Compared with BC, the micropore volume and mesopore volume of KOH-BC increased. The micropore volume of $ZnCl_2$-BC increased observably while the mesopore volume decreased. The total pore volume of $AlCl_3$-BC mesopores had a significant increase. The increase in the number of mesopores could make it easier for the pollutant THPC to enter the pores of the adsorbent, promote the intraparticle diffusion rate, and provide more adsorption sites for THPC. When the average pore size was less than 1.7 times of the second broad dimension of the molecule [38], the target pollutant could not be readily adsorbed because of the size exclusion effect. Using the density functional theory of Gaussian software to optimize the structure of the THPC molecule, the sizes of the THPC molecules were 8.877, 7.643, and 7.063 Å, respectively, while the average sizes of the four materials were larger than 1.7 times that of the THPC molecule, indicating that four materials were in favor of the adsorption.

The functional groups of BC, KOH-BC, $AlCl_3$-BC and $ZnCl_2$-BC were characterized by FTIR, as illustrated in

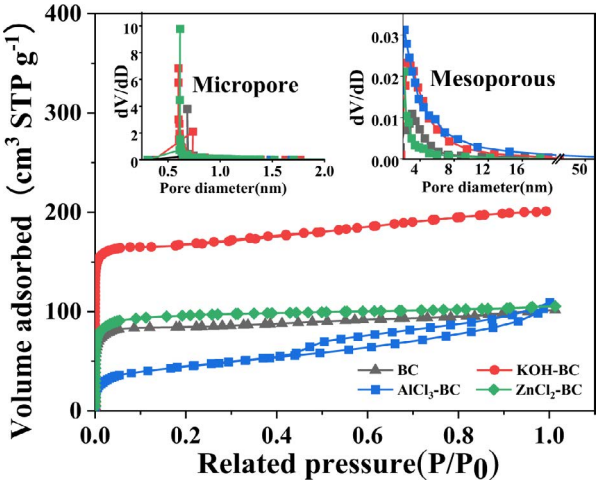

Fig. 2. N_2 adsorption–desorption isotherms and corresponding pore-size distribution curves (inset) of samples.

Table 1
Parameters of surface area and pore structure on samples

Samples	S_{BET} ($m^2 \cdot g^{-1}$)	V_{total} ($cm^3 \cdot g^{-1}$)	V_{mes} ($cm^3 \cdot g^{-1}$)	V_{mic} ($cm^3 \cdot g^{-1}$)	d_P (nm)
BC	261.47	0.16	0.04	0.11	2.41
KOH-BC	512.26	0.31	0.09	0.21	2.43
$AlCl_3$-BC	153.68	0.17	0.14	0.01	4.39
$ZnCl_2$-BC	306.53	0.16	0.03	0.14	2.13

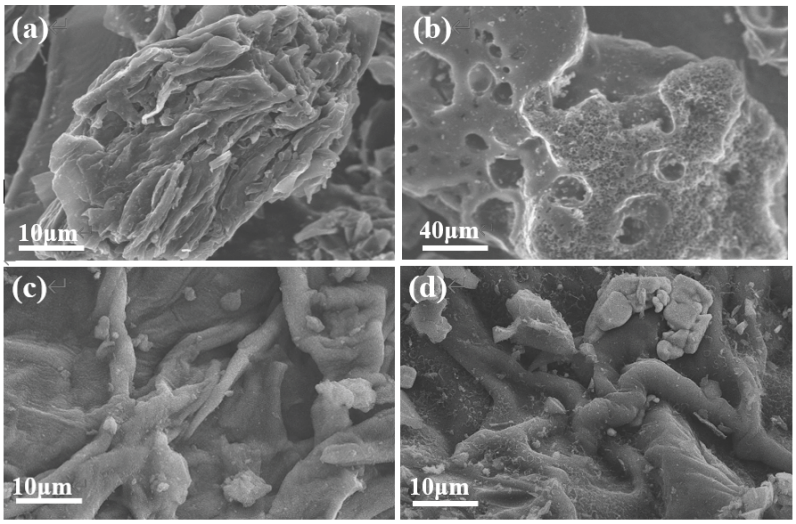

Fig. 1. Scanning electron microscopy images of the BC (a), KOH-BC (b), $AlCl_3$-BC (c), and $ZnCl_2$-BC (d).

Fig. 3. The peak at 3,432 cm^{-1} was the stretching vibration of –OH [25], which may be caused by the water molecules adsorbed on the material. The positions of 2,920 [39] and 2,858 cm^{-1} [34] represented the asymmetric stretching vibration peak of $–CH_3$ and $–CH_2$, respectively. After the activation of KOH, the vibrations of these two vibrational peaks were weakened [40], which might be due to that KOH with high pyrolytic temperature promoted the dehydrogenation and deoxygenation of the products in the biomass pyrolysis reaction and the lost of alkane groups [41], causing the stronger aromaticity of KOH-BC than that of BC. In addition, it might be the stretching vibrations of C=O near 1625 cm^{-1} [42], indicating that there were oxygen-containing functional groups such as carboxyl, carbonyl and ester groups in the materials [39]. After the adsorption of THPC, the C=O vibrational frequencies of the four materials were reduced, which may be attributed to the formation of hydrogen bonds between the carbonyl groups of the materials and the hydroxyl groups of THPC. The stretching vibration frequency of carbonyl groups was reduced for the formation of hydrogen bonds by averaging the electron cloud density. The stretching vibration near 1450 cm^{-1} and the symmetric stretching vibration at 1057 cm^{-1} are C=C and C–O–C, respectively [43].

The XRD of the BC, KOH-BC, $AlCl_3$-BC and $ZnCl_2$-BC are described in Fig. 4. The peaks at 2θ = 29.714°, 31.846°, 36.310°, 39.810°, 43.601°, 47.619°, 48.127° and 58.009° were indexed as (104) (006) (110) (113) (202) (024) (018) and (122) planes, respectively, corresponding to the $CaCO_3$ crystal on the PDF card (01-070-0096). Pomelo peel contains Ca, which is converted into $CaCO_3$ in biomass pyrolysis process. Compared with BC, the diffraction peaks of $CaCO_3$ were enhanced in KOH-BC, which might be due to the crystallinity of $CaCO_3$ crystals that activated KOH could enhance. The diffraction peaks at 2θ = 28.415°, 40.620°, and 66.571° corresponded to the (200) (220) (420) crystal planes of the KCl crystal on the PDF card (01-072-1540). And the diffraction peaks of 2θ = 31.850°, 34.552°, 36.358°, 47.698°, 56.751°, 63.093°, 66.565°, 68.168° 69.291°, 72.876° and 77.214° corresponded to (100) (002) (101) (102) (110) (103) (200) (112) (201) (004) and (202) crystal planes of ZnO crystal on the PDF card (01-070-0096), respectively. The Al peaks of $AlCl_3$-BC in the XRD pattern did not appear, which could be because alumina existed in a weakly crystalline or amorphous form, so XRD could not be effectively detected [44]. When 2θ was at around 23° and 43°, four materials had two relatively broad diffraction peaks, which represented the (002) and (100) crystal planes of turbostratic graphite, which was the characteristic of amorphous carbon [25].

The zeta potential distribution curves of the BC, KOH-BC, $AlCl_3$-BC and $ZnCl_2$-BC are described in Fig. 5. As shown in Fig. 5, the zero-point charges of BC, KOH-BC and $ZnCl_2$-BC was about 2, and the zero-point charge of $AlCl_3$-BC were about 3. The pH of the diluted solution of THPC used in this experiment was all acidic (pH = 3), and the zeta potential of the four kinds of adsorption materials was close to 0 mV at pH = 3, so the electrostatic attraction between the four kinds of biochars and $(HOCH_2)_4P^+$ in aqueous solution can be ignored, indicating that electrostatic attraction was not the main adsorption mechanism of the four kinds of biochar.

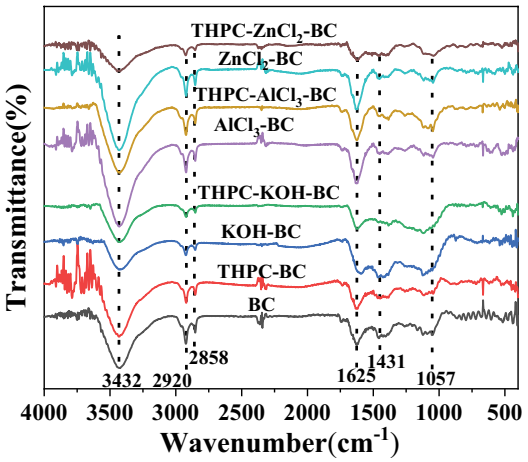

Fig. 3. Fourier-transform infrared spectra of samples and samples after adsorption of THPC.

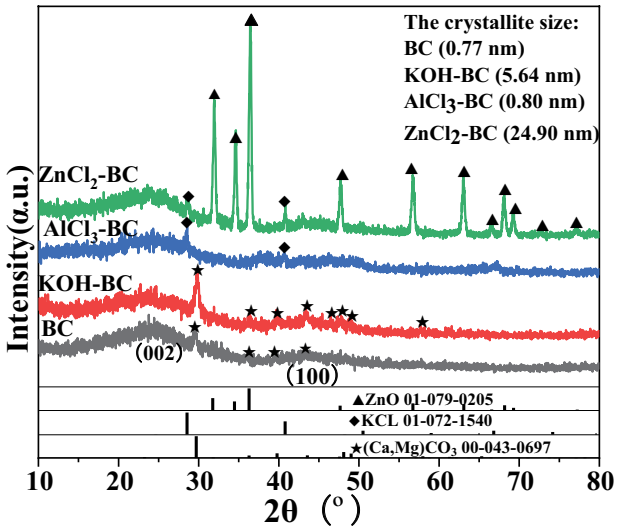

Fig. 4. X-ray diffraction patterns of samples.

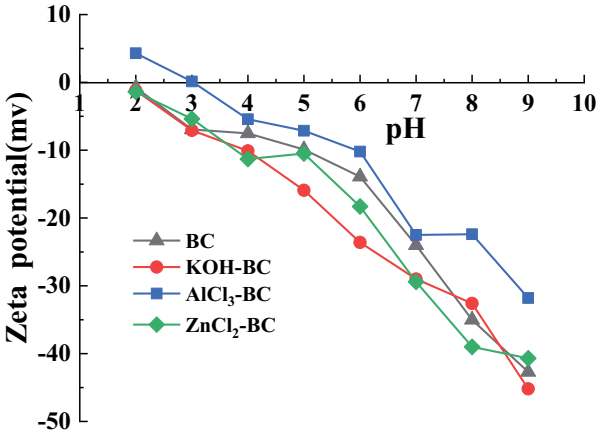

Fig. 5. Zeta potential of samples.

The amount of active substance THPC increases with the pH value increasing (>3), causing the deformation of THPC. Under alkaline conditions, THPC can be decomposed into tris(methyl)phosphine, CH_2O and HCl, among which CH_2O and HCl can form bis(chloromethyl)ether and [45]. Therefore, based on the characteristic of THPC, the influence of pH wasn't explored in the subsequent adsorption experiments.

3.2. Adsorption kinetics model

The adsorption of THPC on BC, KOH-BC, $AlCl_3$-BC and $ZnCl_2$-BC at different times are illustrated in Fig. 6. It can be detected that the adsorption capacities of KOH-BC (230 mg·g^{-1}), $AlCl_3$-BC (184 mg·g^{-1}), and $ZnCl_2$-BC (159 mg·g^{-1}) were increased in comparison with BC (141 mg·g^{-1}). On account of large number of active sites in the materials, the adsorption performance of four materials were very high in the initial time of adsorption (0–60 min). From 60 to 540 min, the adsorption rate was significantly slowed down because most of the adsorption active sites of the materials had been filled as time went on. Until the adsorption rate approached zero at about 720 min, the adsorption capacity tended to be saturated.

In order to further explore the adsorption kinetics and mechanism of THPC on samples, the data in Fig. 6 were fitted and analyzed by three adsorption kinetic models.

The Lagergren first-order model [46] is shown in Eq. (3):

$$\log\left(q_e - q_t\right) = \log q_e - \frac{k_1}{2.303} \tag{3}$$

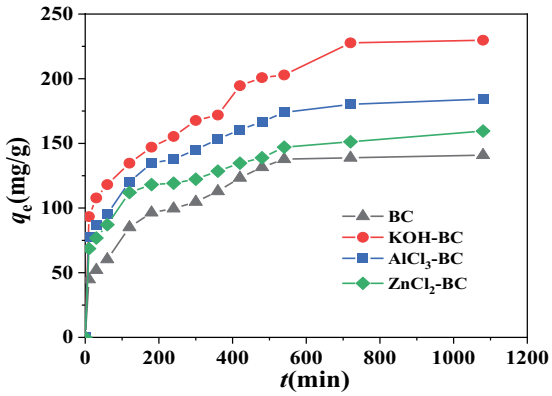

Fig. 6. Adsorption of THPC onto samples at different adsorption time (0.1 g of dosage, pH = 3, T = 298.15 K)

where q_t represents the adsorption capacity at time t, mg·g^{-1}; k_1 belongs to the Lagergren first-order adsorption rate constant, min^{-1}.

The second-order kinetics is shown in Eq. (4):

$$\frac{t}{q_t} = \frac{1}{k_2 q_e^2} + \frac{1}{q_e} t \tag{4}$$

where k_2 stands for the second-order adsorption rate constant, g·(mg·min)$^{-1}$.

The intraparticle diffusion kinetics [47] is shown in Eq. (5):

$$q_t = k_{id} t^{1/2} + C \tag{5}$$

where k_{id} represents the intraparticle diffusion rate constant, mg·g^{-1}·min$^{-1/2}$; C is the intercept.

The relevant parameters of three models are presented in Table 2. As presented in Table 2, R^2 of the second-order kinetic equations for the four materials was higher than that of other kinetics, thus the adsorption of THPC on the four materials was more in line with the second-order kinetic model. And the second-order kinetics fitting diagram was described in Fig. 7. As displayed, all data points did not form a straight line through the origin, which indicated that intraparticle diffusion was not the only rate-determining step.

The fitting diagram of the intraparticle diffusion model of the four materials is shown in Fig. 8, from which each

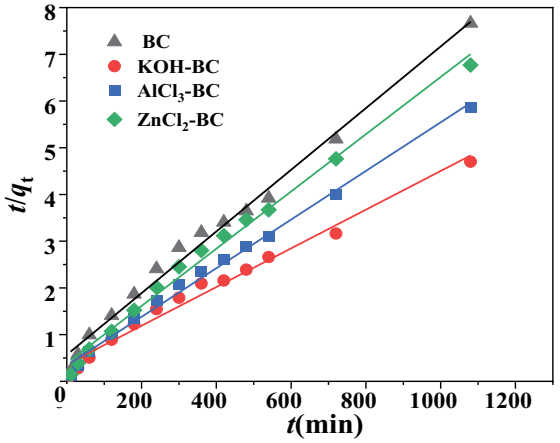

Fig. 7. Second-order kinetics equation plot of THPC on samples (0.1 g of dosage, pH = 3, T = 298.15 K, t = 720 min).

Table 2
Kinetic model models parameters

Adsorbents	Lagergren first-order model			Second-order model			Intraparticle diffusion model		
	k_1 (min^{-1})	$q_{e,c}$ (mg·g^{-1})	R^2	k_2 (min^{-1})	$q_{e,c}$ (mg·g^{-1})	R^2	R_2^2	$k_{id,2}$ (mg·g^{-1}·min$^{-1/2}$)	C_2
BC	5.5×10^{-3}	124.6120	0.9314	7.7×10^{-5}	151.5152	0.9895	0.9877	4.6255	28.83
KOH-BC	4.7×10^{-3}	189.1516	0.8269	4.7×10^{-5}	241.5459	0.9858	0.9879	5.501	74.94
$AlCl_3$-BC	4.3×10^{-3}	119.7485	0.9751	8.0×10^{-5}	192.3077	0.9936	0.9901	4.8068	62.95
$ZnCl_2$-BC	3.2×10^{-3}	86.6483	0.9702	9.7×10^{-5}	163.1321	0.9918	0.9641	3.7067	60.64

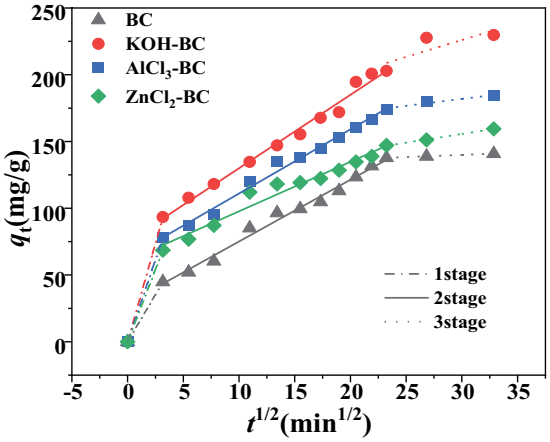

Fig. 8. Intraparticle diffusion models of THPC on samples (0.1 g of dosage, pH = 3, T = 298.15 K, t = 720 min).

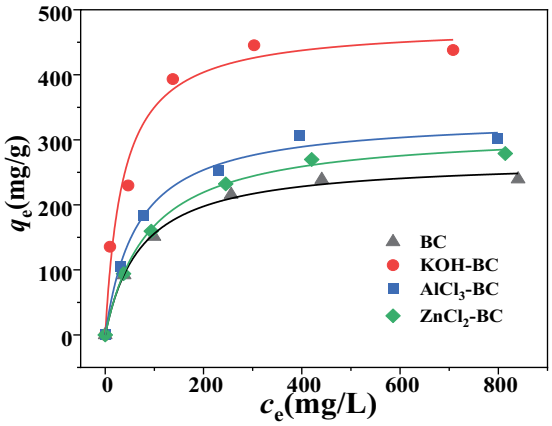

Fig. 9. Adsorption isotherms of THPC on samples (0.1 g of dosage, pH = 3, T = 298.15 K, t = 720 min).

kinetic curve was divided into three linear parts [47], indicating that three distinct sequential kinetic steps were involved. The first stage represented the rapid diffusion process of THPC to the outer surface of the biochar. In the second, the diffusion of THPC in the biochar was expressed, and this step was the rate-limiting step. Thirdly, it described the adsorption–desorption equilibrium stage [48]. As shown in Table 2, the intragranular diffusion rate ($k_{id,2}$) of KOH-BC and $AlCl_3$-BC increased, compared with BC, while that of $ZnCl_2$-BC decreased, which might be due to the decrease of mesopores and the increase of micropores for the $ZnCl_2$-BC. This indicated that the biochar treated by KOH and $AlCl_3$ accelerated the process of intragranular diffusion, while the sample treated by $ZnCl_2$ slowed down the process of intragranular diffusion.

3.3. Adsorption isotherm model

As shown in Fig. 9, when the concentration did not change, the adsorption of KOH-BC on THPC was greatly improved, compared with BC, $AlCl_3$-BC and $ZnCl_2$-BC. In addition, the change in the initial concentration had a great impact on the adsorption of THPC on samples. With C_e increased, the adsorption performance of materials would improve rapidly at first, and then the speed of adsorption decreased due to the limited adsorption active sites until more target pollutants could not be filled to reach equilibrium.

Based on the data in Fig. 9, three adsorption isotherm models, including Langmuir adsorption isotherm model, Freundlich adsorption isotherm model and Dubinin–Radushkevich isotherm model were used to explain the adsorption phenomenon of target pollutants THPC on the prepared samples.

The Langmuir model [46] is given in Eq. (6):

$$\frac{1}{q_e}=\frac{1}{Q_0}+\left(\frac{1}{bQ_0}\right)\left(\frac{1}{C_e}\right) \tag{6}$$

where Q^0 means the unit saturated adsorption capacity when forming a monolayer adsorption, mg·g^{-1}; b is the constant.

The Freundlich model is represented by Eq (7):

$$\log q_e=\log K_F+\frac{1}{n}\log C_e \tag{7}$$

where K_F and n are adsorption constants.

The Dubinin–Radushkevich isotherm model is represented in Eqs. (8)–(10):

$$\ln q_e=\ln q_m-K_D\varepsilon^2 \tag{8}$$

$$\varepsilon=RT\ln\left(1+\frac{1}{C_e}\right) \tag{9}$$

$$E=\frac{1}{\sqrt{2K_D}} \tag{10}$$

where q_m is monolayer saturated adsorption capacity, mol·g^{-1}; K_D is adsorption constant related to average free energy, mol^2·(kJ^2)$^{-1}$; ε is adsorption potential; E is adsorption free energy, kJ·mol^{-1}; R is a thermodynamic constant, 8.314 J·(K·mol)$^{-1}$.

The fitting parameters of three models are shown in Table 3, from which the adsorption of THPC by BC, KOH-BC, $AlCl_3$-BC and $ZnCl_2$-BC was more consistent with the Langmuir model, that is, the adsorption process of the four materials on THPC was monolayer adsorption.

The fitting diagram of the Langmuir model is shown in Fig. 10. According to the parameters of Dubinin–Radushkevich isothermal adsorption model, the values of E, the adsorption free energy of four materials adsorbing THPC, is less than 16 at 25°C, which indicated that at this temperature, the adsorption of THPC by the four materials was mainly ion exchange adsorption and $(HOCH_2)_4P^+$ might be ion exchange adsorption of Ca^+, K^+, Mg^{2+} cations on biochar.

3.4. Adsorption thermodynamics of biochar adsorption of THPC

Thermodynamic parameters for THPC adsorption on BC, KOH-BC, $AlCl_3$-BC and $ZnCl_2$-BC were calculated using Eqs. (11)–(13) [47,49].

Table 3
Isotherm models parameters

Adsorbents	Langmuir			Freundlich				Dubinin–Radushkevich		
	Q^0 (mg·g^{-1})	b (L·mg^{-1})	R^2	K_F	N	R^2	q_m (mol·g^{-1})	K_D (mol^2·(g^2)$^{-1}$)	E (kJ·mol^{-1})	R^2
BC	271.0027	0.0133	0.9977	32.0605	2.6749	0.9690	0.0028	0.0038	11.4679	0.9429
KOH-BC	416.6667	0.0485	0.9480	74.7567	3.3638	0.9200	0.0049	0.0049	12.5992	0.9499
$AlCl_3$-BC	338.9831	0.0148	0.9969	38.9063	3.0324	0.9106	0.0037	0.0038	11.4403	0.9429
$ZnCl_2$-BC	314.4654	0.0115	0.9989	28.5851	2.7705	0.9338	0.0036	0.0042	10.8589	0.9618

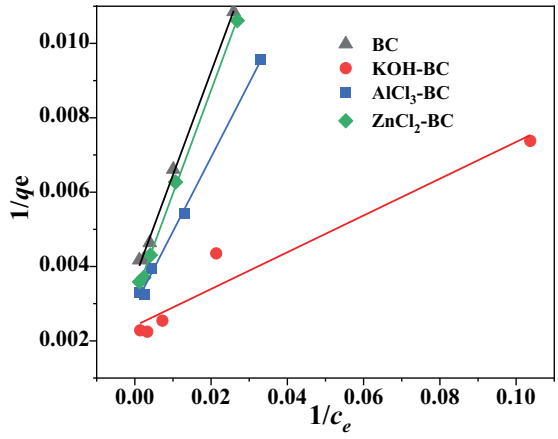

Fig. 10. Langmuir adsorption isotherms of THPC on sample (0.1 g of dosage, pH = 3, T = 298.15 K, t = 720 min).

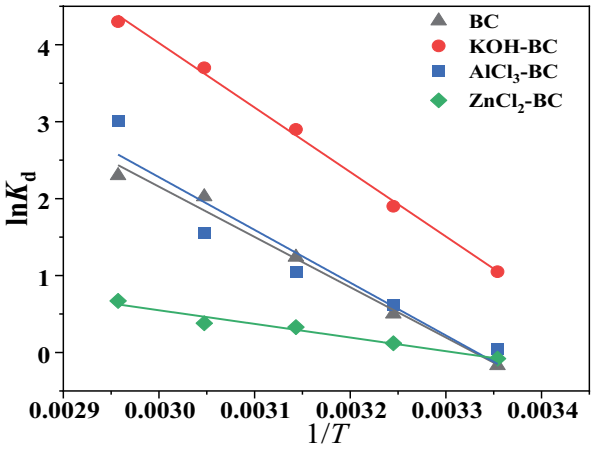

Fig. 11. The logK_d ~ 1/T relation diagram of THPC adsorbed by samples (0.1 g of dosage, pH = 3, t = 720 min).

$$G = \Delta H - T\Delta S \tag{11}$$

$$K_d = \frac{Q_e}{C_e} \tag{12}$$

$$\ln K_d = \frac{\Delta S}{R} - \frac{\Delta H}{RT} \tag{13}$$

where ΔG is the Gibbs free energy change, J·mol^{-1}; ΔH is the adsorption enthalpy change, J·mol^{-1}; ΔS is the adsorption entropy change, J·(K·mol)$^{-1}$; K_d is the distribution coefficient.

The logK_d ~ 1/T diagram and the thermodynamic parameters of the adsorption process of THPC are displayed in Fig. 11 and Table 4, respectively. As can be seen from Table 4, the value of ΔH was positive in the process of the adsorption of THPC by each material, that is, the reaction of adsorption was an endothermic reaction. A positive value of ΔS expressed that the degree of freedom of system chaos increased during the adsorption process, and a spontaneous process was obtained with a negative value of ΔG in the adsorption process of THPC. In summary, the adsorption process of THPC was a spontaneous endothermic reaction.

3.5. Compared with other adsorbents

There are very few studies on the adsorption of THPC in other literature. Therefore, in order to compare the adsorption effects of other adsorption materials on THPC, four types of biochar, BC, KOH-BC, $AlCl_3$-BC and $ZnCl_2$-BC in

Table 4
Thermodynamic parameters

Adsorbents	T (K)	ΔG (kJ·mol^{-1})	ΔH (kJ·mol^{-1})	ΔS (kJ·(K·mol)$^{-1}$)
BC	298.15	–0.20	54.34	0.18
	308.15	–2.03		
	318.15	–3.85		
	328.15	–5.68		
	338.15	–7.51		
KOH-BC	298.15	–2.19	69.70	0.24
	308.15	–4.60		
	318.15	–7.01		
	328.15	–9.42		
	338.15	–11.83		
$AlCl_3$-BC	298.15	–0.01	57.01	0.19
	308.15	–1.92		
	318.15	–3.83		
	328.15	–5.74		
	338.15	–7.65		
$ZnCl_2$-BC	298.15	–0.13	14.74	0.05
	308.15	–0.63		
	318.15	–1.13		
	328.15	–1.63		
	338.15	–2.13		

this study were compared with other adsorption materials prepared in the same laboratory for THPC adsorption performance. As shown in Table 5, compared with the other adsorbents prepared, the four types of biochar prepared in this article have a high adsorption capacity for THPC. Besides, they are stable, inexpensive and have good environmental compatibility, thus can be used to remove THPC from industrial wastewater.

3.6. Possible adsorption mechanism

The Brunauer–Emmett–Teller test showed that the number of micropores and mesopores increased in the biochar when KOH was activated. More mesopores were generated by the co-pyrolysis of $AlCl_3$ and biochar, and the number of micropores was greatly increased due to the reduction of mesopores in $ZnCl_2$-BC. The batch adsorption experiments showed that KOH-BC, $AlCl_3$-BC and $ZnCl_2$-BC had higher adsorption capacities of THPC than BC, with which KOH-BC having the best adsorption capacity. Pore-filling was more likely to be occur on adsorbents with porous structures and the large specific surface area as well as abundant pore structure on biochar provided more adsorption sites for the adsorption of THPC, which had a greater effect on the adsorption performance of THPC.

Oxygen-containing functional groups in the biochar could interact with positively charged hydrophilic organic compounds to generate hydrogen bonding forces by generating strong π-H forces [50]. As can be seen from FTIR, the existence of many oxygen-containing functional groups in the heterogeneous carbonaceous materials of the four materials made it very possible to form hydrogen bonds, which can equalize the density of the electron cloud, thus reducing the vibration frequency of the negatively charged C=O group. The C=O vibrations of the materials after adsorption of THPC were weakened, indicating that the hydrogen bonding forces were produced by the C=O groups on biochar and THPC.

In addition, with the biochar as an electron donor and the cationic $(HOCH_2)_4P^+$ as an electron acceptor [51], a cation-π interaction occurred between the $(HOCH_2)_4P^+$ cation and the biochar aromatic ring. The cationic-π interaction, which depended on the degree of aromaticity of biochar [52],was an important mechanism for biochar adsorption of $(HOCH_2)_4P^+$ cations. The more conjugated aromatic structures there were, the stronger the electron-donating ability there was and the more obvious the cation-π effect there was.

Biochar is rich in cations. XRD showed that biochar contained K^+, Na^+ and Mg^{2+} ions, which could be exchanged with $(HOCH_2)_4P^+$. The Dubinin–Radushkevich isothermal model showed that there might be ion exchange when biochar adsorbed THPC.

Above all, the main adsorption mechanisms of THPC removal by BC, KOH-BC, $AlCl_3$-BC and $ZnCl_2$-BC included pore-filling, cation-π interactions, hydrogen bonding and ion exchange, the diagram of which is displayed in Fig. 12.

4. Antibacterial activity

4.1. Effects of contact time on antibacterial activity

The antibacterial activities of BC and KOH-BC on *E. coli* after adsorption of THPC were explored, using BC and KOH-BC with the best adsorption performance on THPC after activation as the research objects. The effects of THPC-BC and THPC-KOH-BC on the antibacterial activity of *E. coli* are shown in Figs. 13 and 14, respectively.

After only 1 h contact with the *E. coli* dilution, 100% of the *E. coli* was killed by THPC-KOH-BC under the same dosage, while THPC-BC still had a small amount of surviving *E. coli*

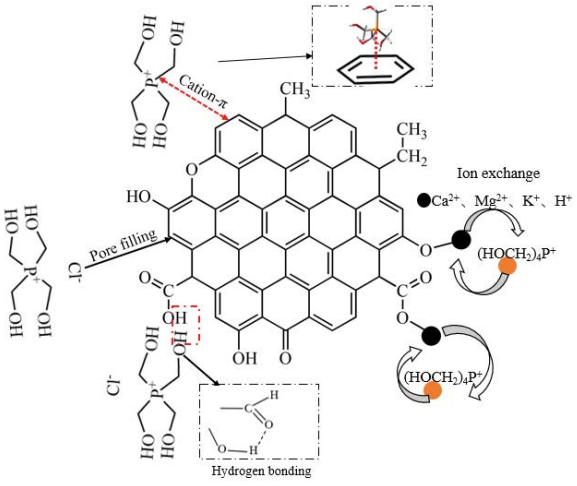

Fig. 12. Possible adsorption mechanism.

Table 5
Comparison of THPC adsorption performance between BC, KOH-BC, $AlCl_3$-BC, $ZnCl_2$-BC and other materials

Adsorbents	Maximum adsorption capacity ($mg \cdot g^{-1}$)	Characteristics of materials
BC	140.90	Stable structure, cheap raw materials and good environmental compatibility; but tube furnace pyrolysis takes a long time
KOH-BC	229.75	
$AlCl_3$-BC	184.29	
$ZnCl_2$-BC	159.50	
Microwave biochar	45.86	Fast preparation speed, but small specific surface area, poor adsorption effect on THPC
NiFe-LDH	40.50	Unstable under acidic conditions
Ce-MOF	81.00	Unstable under acidic conditions, high preparation cost
Graphene oxide	142.97	High preparation cost

after the same contact time. It can be seen from the adsorption experiments that the amount of THPC adsorbed by KOH-BC was much larger than BC. so that the sterilization effect of THPC-KOH-BC was better than that of THPC-BC. As shown in Figs. 13b and 14b, under the same conditions, the BC before adsorption contacted with *E. coli* for 1 h performed no bactericidal effect, and the amount of *E. coli* was reduced due to a fraction of the bacteria entered the biochar pore, which resulted in fewer *E. coli* to be detected in the supernatant of *E. coli* solution.

4.2. Bacteriostatic kinetics

Generally, the logarithm of bacterial reduction and the contact time between bacteriostatic substance and bacterial solution are used as ordinate and abscissa, respectively, to obtain the survival curve of bacteria. Ideally, the inactivation of bacteria caused by chemical bacteriostatic agents were to follow the first-order log-linear model, which shows that there was a linear relationship between the time of bacteriostatic substances acting on bacteria and the logarithmic value of bacteria reduction [53]. The first-order log-linear model is represented in Eq. (14):

$$\log\frac{N_t}{N_0} = -\frac{t}{D} + C \tag{14}$$

where N_t is the concentration of *E. coli* in the supernatant at t min, CFU/mL; N_0 is the initial microbial concentration without adding bacteriostatic substances, CFU/mL; D is the time required to reduce live bacteria by 90%, min; C is the intercept of the linear model.

In some cases, the first-order log-linear model is not applicable, and the nonlinear model needs to be used. The Weibull model takes the killing of *E. coli* as the probability event, which is related to the heterogeneity of the bacterial population. The Weibull model is expressed in Eq. (15):

$$\log\frac{N_t}{N_0} = -b \times t^n \tag{15}$$

where b and n are the scale factor shape parameters related to temperature and pressure, respectively.

The fitting parameters of the two models were shown in Table 6 and the fitting diagrams of the two models are shown in Figs. 15 and 16, respectively. It can be seen from Table 6 that the bacteriostatic kinetics of THPC-BC on *E. coli* conformed to the first-order log-linear model, while the bacteriostatic kinetics of THPC-KOH-BC on *E. coli* conformed to the Weibull model. According to the parameters simulated by the first-order log-linear model, the time required to reduce the surviving bacteria by 90% of *E. coli* was 48.38 min for THPC-BC and 15.34 min for THPC-KOH-BC. According to the related parameters of the Weibull model, the parameter n of THPC-BC and THPC-KOH-BC was less than 1, indicating that the inactivation curves of THPC-BC and THPC-KOH-BC to *E. coli* were both of the downward concave type.

4.3. Bacteriostasis mechanism

As shown in Fig. 17, THPC was released into the bacterial liquid in the suspension of *E. coli* after the adsorption by biochar. THPC is a kind of quaternary phosphine salt, which is often used as a non-oxidizing fungicide in industrial water treatment. Non-oxidizing fungicides act on special parts of microorganisms, so they are not affected by

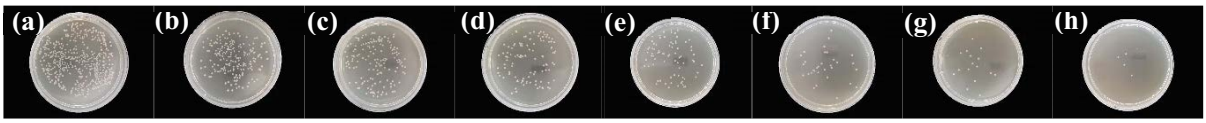

Fig. 13. Effect of contact time between THPC-BC and *Escherichia coli* on antibacterial activity (a) blank control, (b) only BC, (c) 10 min, (d) 20 min, (e) 30 min, (f) 40 min, (g) 60 min, and (h) 90 min.

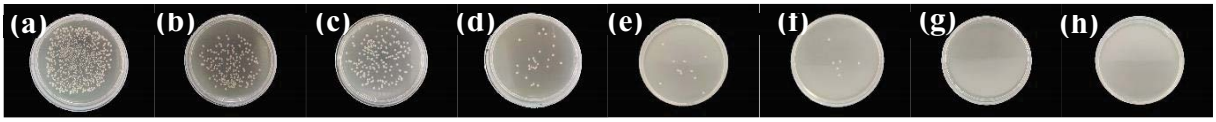

Fig. 14. Effect of contact time between THPC-KOH-BC and *Escherichia coli* on antibacterial activity (a) blank control, (b) only BC, (c) 10 min, (d) 20 min, (e) 30 min, (f) 40 min, (g) 60 min, and (h) 90 min.

Table 6
Fitting parameters of the first-order log-linear model and the Weibull model of THPC-BC and THPC-KOH-BC

Materials	First-order log-linear model					Weibull model				
	D (min)	$-C$	R^2	RMSE	SSE	B	N	R^2	RMSE	SSE
THPC-BC	48.38	0.3792	0.9881	0.0741	0.0220	0.1013	0.6829	0.9810	0.0939	0.0353
THPC-KOH-BC	15.24	0.1868	0.9561	0.2221	0.0987	0.1214	0.8483	0.9651	0.1982	0.0785

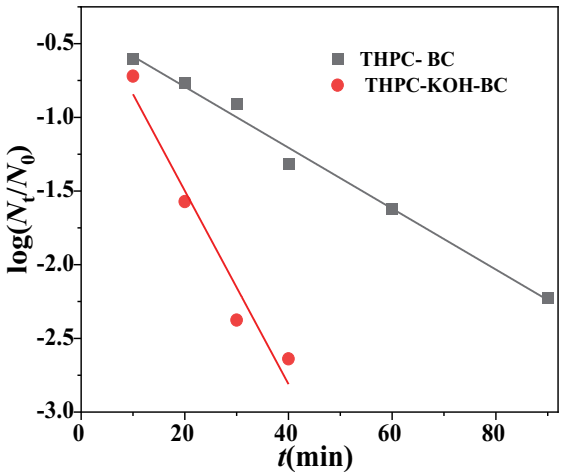

Fig. 15. Fitting diagram of the first-order log-linear model.

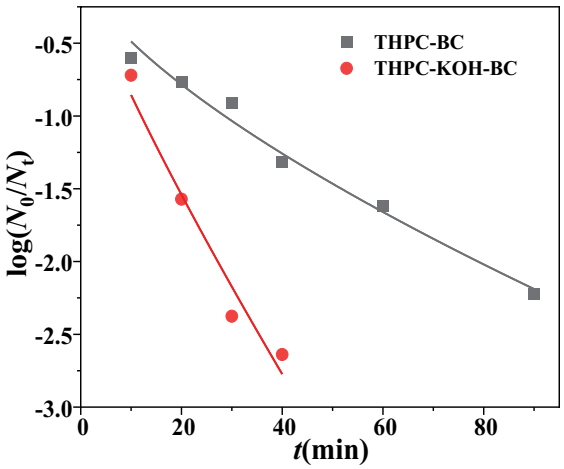

Fig. 16. Fitting diagram of the Weibull model.

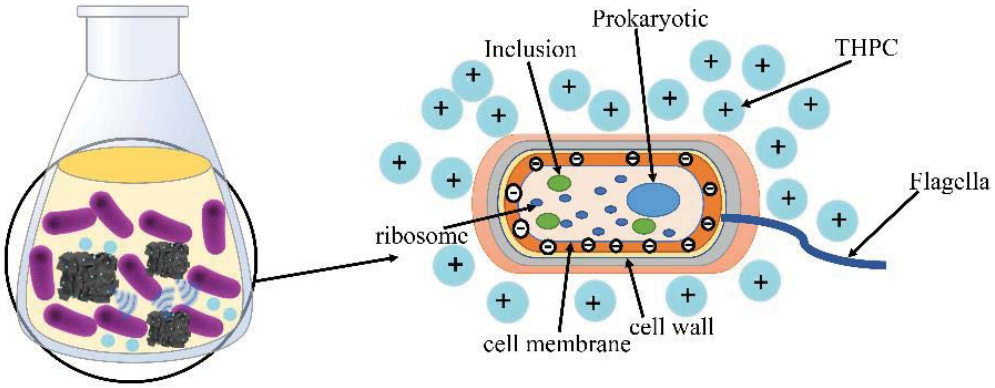

Fig. 17. Bacteriostasis mechanism.

reducing substances in water. The quaternary phosphine atom in THPC has a positive charge and can be adsorbed on the negatively charged bacteria, resulting in an imbalance of negative charge on the cell surface of the bacteria with cell degeneration, rupture, and leakage of cell contents, thus achieving the effect of sterilization.

5. Conclusion

KOH-BC, $AlCl_3$-BC and $ZnCl_2$-BC were prepared by the co-pyrolysis of activators with waste pomelo peel, a waste of agriculture and forestry. The adsorption capacities of activated-BC were higher than that of original BC. The adsorption of THPC by the four materials accorded with the second-order kinetics and the Langmuir adsorption isotherm model, indicating that the adsorption process was monolayer adsorption. Besides, intraparticle diffusion was not the only rate control step. Thermodynamic parameters show that the adsorption processes were both spontaneous and endothermic. The main adsorption mechanisms, including pore filling, cation-π interaction, hydrogen bonding, and ion exchange, can be concluded from the experiment. The modified biochar KOH-BC effectively absorbed and recovered THPC from wastewater, which gave KOH-BC an excellent bactericidal effect on *E. coli* after adsorption of THPC. Therefore, biochar after THPC adsorption can be used as sterilization material, especially for sterilization of lake bottom mud, industrial sludge, and industrial garbage, which provides a new idea for THPC emission reduction and resource utilization but also has a certain practical value at a low cost.

Statements and declarations

Ethics approval: We assured that this manuscript is original work and this work neither accepted nor submitted simultaneously to any other journals.

Funding: This study was financially supported by the Key R&D plan of Shaanxi Province China (2022SF-578).

Declaration of interests: The authors declare that they have no known competing financial interests or personal relationships that could have appeared to influence the work reported in this paper.

References

[1] A.M. Awad, S.M.R. Shaikh, R. Jalab, M.H. Gulied, M.S. Nasser, A. Benamor, S. Adham, Adsorption of organic pollutants by natural and modified clays: a comprehensive review,

Sep. Purif. Technol., 228 (2019) 115719, doi: 10.1016/j.seppur.2019.115719.
[2] D.B. Miklos, C. Remy, M. Jekel, K.G. Linden, J.E. Drewes, U. Hubner, Evaluation of advanced oxidation processes for water and wastewater treatment - a critical review, Water Res., 139 (2018) 118–131.
[3] A.A. Alqadami, S.M. Wabaidur, B.-H. Jeon, M.A. Khan, Co-hydrothermal valorization of food waste: process optimization, characterization, and water decolorization application, Biomass Conver. Biorefin., (2023) 1–12, doi: 10.1007/s13399-022-03711-7.
[4] I. Ali, O.M.L. Alharbi, Z.A. Alothman, A.M. Al-Mohaimeed, A. Alwarthan, Modeling of fenuron pesticide adsorption on CNTs for mechanistic insight and removal in water, Environ. Res., 170 (2019) 389–397.
[5] D.V. Moiseev, B.R. James, Syntheses and rearrangements of tris(hydroxymethyl)phosphine and tetrakis(hydroxymethyl) phosphonium salts, Phosphorus, Sulfur Silicon Relat. Elem., 195 (2020) 687–712.
[6] B. Zhao, T.J. Kolibaba, S. Lazar, J.C. Grunlan, Environmentally-benign, water-based covalent polymer network for flame retardant cotton, Cellulose, 28 (2021) 5855–5866.
[7] S.X. Shao, L. Jiang, Y. Li, K.Q. Shi, Effect of pH on the phosphorous components in tetra-hydroxymethyl phosphonium chloride solution, Adv. Mater. Res., 560 (2012) 237–241.
[8] D.V. Moiseev, B.R. James, Tetrakis(hydroxymethyl) phosphonium salts: their properties, hazards and toxicities, Phosphorus, Sulfur Silicon Relat. Elem., 195 (2019) 263–279.
[9] S. Liu, H. Zheng, T. Li, Degradation characteristics and microbial community of phosphine biopurification systems, Environ. Eng. Sci., 38 (2021) 802–810.
[10] W.-C. Shao, H. Wu, A. Shiue, C.-H. Tseng, Y.-W. Wang, C.-F. Hsu, G. Leggett, Chitosan-dosed adsorptive filter media for removal of formaldehyde from indoor air - performance and cancer risk assessment, Chem. Phys. Lett., 779 (2021) 138836, doi: 10.1016/j.cplett.2021.138836.
[11] F. Liu, J. Cao, Z. Yang, W. Xiong, Z. Xu, P. Song, M. Jia, S. Sun, Y. Zhang, X. Zhong, Heterogeneous activation of peroxymonosulfate by cobalt-doped MIL-53 (Al) for efficient tetracycline degradation in water: coexistence of radical and non-radical reactions, J. Colloid Interface Sci., 581 (2021) 195–204.
[12] P. Krzeminski, C. Schwermer, A. Wennberg, K. Langford, C. Vogelsang, Occurrence of UV filters, fragrances and organophosphate flame retardants in municipal WWTP effluents and their removal during membrane post-treatment, J. Hazard. Mater., 323 (2017) 166–176.
[13] A.V. Sviridov, T.V. Shushkova, D.O. Epiktetov, S.V. Tarlachkov, I.T. Ermakova, A.A. Leontievsky, Biodegradation of organophosphorus pollutants by soil bacteria: biochemical aspects and unsolved problems, Appl. Biochem. Microbiol., 57 (2021) 836–844.
[14] X. Huang, L. Huang, S.R. Babu Arulmani, J. Yan, Q. Li, J. Tang, K. Wan, H. Zhang, T. Xiao, M. Shao, Research progress of metal organic frameworks and their derivatives for adsorption of anions in water: a review, Environ. Res., 204 (2022) 112381–112381.
[15] H.A. Murad, M. Ahmad, J. Bundschuh, Y. Hashimoto, M. Zhang, B. Sarkar, Y.S. Ok, A remediation approach to chromium-contaminated water and soil using engineered biochar derived from peanut shell, Environ. Res., 204 (2022) 112125, doi: 10.1016/j.envres.2021.112125.
[16] A. Othmani, S. Magdouli, P.S. Kumar, A. Kapoor, P.V. Chellam, O. Gokkus, Agricultural waste materials for adsorptive removal of phenols, chromium(VI) and cadmium(II) from wastewater: a review, Environ. Res., 204 (2022) 111916, doi: 10.1016/j.envres.2021.111916.
[17] M.-X. Zhan, Y.-W. Liu, W.-W. Ye, T. Chen, W.-T. Jiao, Modification of activated carbon using urea to enhance the adsorption of dioxins, Environ. Res., 204 (2022) 112035, doi: 10.1016/j.envres.2021.112035.
[18] H. Xu, S. Zhu, M. Xia, F. Wang, X. Ju, Three-dimension hierarchical composite via *in-situ* growth of Zn/Al layered double hydroxide plates onto polyaniline-wrapped carbon sphere for efficient naproxen removal, J. Hazard. Mater., 423 (2022) 127192, doi: 10.1016/j.jhazmat.2021.127192.
[19] S. Rezania, A. Mojiri, J. Park, N. Nawrot, E. Wojciechowska, N. Marraiki, N.S.S. Zaghloul, Removal of lead ions from wastewater using lanthanum sulfide nanoparticle decorated over magnetic graphene oxide, Environ. Res., 204 (2022) 111959, doi: 10.1016/j.envres.2021.111959.
[20] J.O. Fernandes, C.A. Rolim Bernardino, C.F. Mahler, R.E. Santelli, B.F. Braz, R.C. Borges, M.C. da Cunha Veloso, G.A. Romeiro, F.H. Cincotto, Biochar generated from agro-industry sugarcane residue by low temperature pyrolysis utilized as an adsorption agent for the removal of thiamethoxam pesticide in wastewater, Water Air Soil Pollut., 232 (2021) 67, doi: 10.1007/s11270-021-05030-5.
[21] J. Hoslett, H. Ghazal, N. Mohamad, H. Jouhara, Removal of methylene blue from aqueous solutions by biochar prepared from the pyrolysis of mixed municipal discarded material, Sci. Total Environ., 714 (2020) 136832, doi: 10.1016/j.scitotenv.2020.136832.
[22] J. Wang, S. Wang, Preparation, modification and environmental application of biochar: a review, J. Cleaner Prod., 227 (2019) 1002–1022.
[23] B. Li, L. Yang, C.-q. Wang, Q.-p. Zhang, Q.-c. Liu, Y.-d. Li, R. Xiao, Adsorption of Cd(II) from aqueous solutions by rape straw biochar derived from different modification processes, Chemosphere, 175 (2017) 332–340.
[24] Q. Yin, R. Wang, Z. Zhao, Application of Mg–Al-modified biochar for simultaneous removal of ammonium, nitrate, and phosphate from eutrophic water, J. Cleaner Prod., 176 (2018) 230–240.
[25] D. Hsu, C. Lu, T. Pang, Y. Wang, G. Wang, Adsorption of ammonium nitrogen from aqueous solution on chemically activated biochar prepared from sorghum distillers grain, Appl. Sci., 9 (2019) 5249, doi: 10.3390/app9235249.
[26] Y.F. Ma, Y. Qi, L. Yang, L. Wu, P. Li, F. Gao, X.B. Qi, Z.L. Zhang, Adsorptive removal of imidacloprid by potassium hydroxide activated magnetic sugarcane bagasse biochar: adsorption efficiency, mechanism and regeneration, J. Cleaner Prod., 292 (2021) 126005, doi: 10.1016/j.jclepro.2021.126005.
[27] Y. Yao, B. Gao, F. Wu, C. Zhang, L. Yang, Engineered biochar from biofuel residue: characterization and its silver removal potential, ACS Appl. Mater. Interfaces, 7 (2015) 10634–10640.
[28] E. Antunes, M.V. Jacob, G. Brodie, P.A. Schneider, Silver removal from aqueous solution by biochar produced from biosolids via microwave pyrolysis, J. Environ. Manage., 203 (2017) 264–272.
[29] Y. Zhou, B. Gao, A.R. Zimmerman, X. Cao, Biochar-supported zerovalent iron reclaims silver from aqueous solution to form antimicrobial nanocomposite, Chemosphere, 117 (2014) 801–805.
[30] Q. Chen, J. Qin, P. Sun, Z. Cheng, G. Shen, Cow dung-derived engineered biochar for reclaiming phosphate from aqueous solution and its validation as slow-release fertilizer in soil crop system, J. Cleaner Prod., 172 (2018) 2009–2018.
[31] B.O. Nardis, J. Santana da Silva Carneiro, I.M.G.D. Souza, R.G.D. Barros, L.C. Azevedo Melo, Phosphorus recovery using magnesium-enriched biochar and its potential use as fertilizer, Arch. Agron. Soil Sci., 67 (2020) 1017–1033.
[32] B. Wang, Y. Ma, X. Lee, P. Wu, F. Liu, X. Zhang, L. Li, M. Chen, Environmental-friendly coal gangue-biochar composites reclaiming phosphate from water as a slow-release fertilizer, Sci. Total Environ., 758 (2021) 143664, doi: 10.1016/j.scitotenv.2020.143664.
[33] C. Schang, A. Lintern, P.L.M. Cook, G. Rooney, R. Coleman, H.M. Murphy, A. Deletic, D. McCarthy, *Escherichia coli* survival and transfer in estuarine bed sediments, River Res. Appl., 34 (2018) 606–614.
[34] L. Liu, Y. Li, S. Fan, Preparation of KOH and H_3PO_4 modified biochar and its application in methylene blue removal from aqueous solution, Processes, 7 (2019) 891, doi: 10.3390/pr7120891.
[35] W. Chen, M. Gong, K. Li, M. Xia, Z. Chen, H. Xiao, Y. Fang, Y. Chen, H. Yang, H. Chen, Insight into KOH activation

mechanism during biomass pyrolysis: chemical reactions between O-containing groups and KOH, Appl. Energy, 278 (2020) 115730, doi: 10.1016/j.apenergy.2020.115730.
[36] Z. Qiu, Y. Wang, X. Bi, T. Zhou, J. Zhou, J. Zhao, Z. Miao, W. Yi, P. Fu, S. Zhuo, Biochar-based carbons with hierarchical micro-meso-macro porosity for high rate and long cycle life supercapacitors, J. Power Sources, 376 (2018) 82–90.
[37] B.M. Al-Shehri, A.E.R.S. Khder, S.S. Ashour, M.S. Hamdy, A review: the utilization of mesoporous materials in wastewater treatment, Mater. Res. Express, 6 (2019) 122002, doi: 10.1088/2053-1591/ab52af.
[38] L. Yan, Y. Liu, Y. Zhang, S. Liu, C. Wang, W. Chen, C. Liu, Z. Chen, Y. Zhang, $ZnCl_2$ modified biochar derived from aerobic granular sludge for developed microporosity and enhanced adsorption to tetracycline, Bioresour. Technol., 297 (2020) 122381, doi: 10.1016/j.biortech.2019.122381.
[39] W. Liu, D. Ren, J. Wu, Z. Wang, S. Zhang, X. Zhang, X. Gong, Adsorption behavior of 2,4-DCP by rice straw biochar modified with CTAB, Environ. Technol., 42 (2021) 3797–3806.
[40] W. Chen, M. Gong, K. Li, M. Xia, Z. Chen, H. Xiao, Y. Fang, Y. Chen, H. Yang, H. Chen, Insight into KOH activation mechanism during biomass pyrolysis: chemical reactions between O-containing groups and KOH, Appl. Energy, 278 (2020) 115730, doi: 10.1016/j.apenergy.2020.115730.
[41] H. Huang, J. Tang, K. Gao, R. He, H. Zhao, D. Werner, Characterization of KOH modified biochars from different pyrolysis temperatures and enhanced adsorption of antibiotics, RSC Adv., 7 (2017) 14640–14648.
[42] J. Li, Q. Li, C. Qian, X. Wang, Y. Lan, B. Wang, W. Yin, Volatile organic compounds analysis and characterization on activated biochar prepared from rice husk, Int. J. Environ. Sci. Technol., 16 (2019) 7653–7662.
[43] C. Yang, S. Miao, T. Li, Influence of water washing treatment on *Ulva prolifera*-derived biochar properties and sorption characteristics of ofloxacin, Sci. Rep., 11 (2021) 1797, doi: 10.1038/s41598-021-81314-4.
[44] J. Liang, Y. Chen, M. Cai, M. Gan, J. Zhu, One-pot pyrolysis of metal-embedded biochar derived from invasive plant for efficient Cr(VI) removal, J. Environ. Chem. Eng., 9 (2021) 105714, doi: 10.1016/j.jece.2021.105714.
[45] D.V. Moiseev, B.R. James, Tetrakis(hydroxymethyl) phosphonium salts: their properties, hazards and toxicities, Phosphorus, Sulfur Silicon Relat. Elem., 195 (2020) 263–279.
[46] Y. Wu, Z. Liu, M.F. Bakhtari, J. Luo, Preparation of GO/MIL-101(Fe,Cu) composite and its adsorption mechanisms for phosphate in aqueous solution, Environ. Sci. Pollut. Res., 28 (2021) 51391–51403.
[47] Y. Mu, W. He, H. Ma, Enhanced adsorption of tetracycline by the modified tea-based biochar with the developed mesoporous and surface alkalinity, Bioresour. Technol., 342 (2021) 126001, doi: 10.1016/j.biortech.2021.126001.
[48] V.-P. Dinh, T.-D.-T. Huynh, H.M. Le, V.-D. Nguyen, V.-A. Dao, N.Q. Hung, L.A. Tuyen, S. Lee, J. Yi, T.D. Nguyen, L.V. Tan, Insight into the adsorption mechanisms of methylene blue and chromium(III) from aqueous solution onto pomelo fruit peel, RSC Adv., 9 (2019) 25847–25860.
[49] Y. Tong, P.J. McNamara, B.K. Mayer, Adsorption of organic micropollutants onto biochar: a review of relevant kinetics, mechanisms and equilibrium, Environ. Sci. Water Res. Technol., 5 (2019) 821–838.
[50] Z. Luo, B. Yao, X. Yang, L. Wang, Z. Xu, X. Yan, L. Tian, H. Zhou, Y. Zhou, Novel insights into the adsorption of organic contaminants by biochar: a review, Chemosphere, 287 (2022) 132113, doi: 10.1016/j.chemosphere.2021.132113.
[51] P. Zhang, H. Sun, C. Ren, L. Min, H. Zhang, Sorption mechanisms of neonicotinoids on biochars and the impact of deashing treatments on biochar structure and neonicotinoids sorption, Environ. Pollut., 234 (2018) 812–820.
[52] L.H. Nguyen, X.H. Nguyen, N.D.K. Nguyen, H.T. Van, V.N. Thai, H.N. Le, V.D. Pham, N.A. Nguyen, T.P. Nguyen, T.H. Nguyen, H_2O_2 modified-hydrochar derived from paper waste sludge for enriched surface functional groups and promoted adsorption to ammonium, J. Taiwan Inst. Chem. Eng., 126 (2021) 119–133.
[53] J. Arora, D. Oudit, J.W. Austin, H.S. Ramaswamy, Evaluation of thermal destruction kinetics of *Clostridium difficile* spores (ATCC 17857) in lean ground beef with first-order/Weibull modeling considerations, J. Food Process Eng., 42 (2019) e13273, doi: 10.1111/jfpe.13273.